Verification of the localized-wave transmission effect

Richard W. Ziolkowski[a] and D. Kent Lewis
University of California, Lawrence Livermore National Laboratory, Livermore, California 94550

(Received 18 June 1990; accepted for publication 16 August 1990)

An acoustic array driven with a designed set of localized-wave (LW) solutions of the scalar-wave equation generates a robust, well-behaved, transient pencil beam of ultrasound in water. The performance of the LW-pulse-driven array theoretically and experimentally exceeds a tenfold improvement over related continuous-wave excitations of the same array.

I. INTRODUCTION

Large classes of nonseparable space-time solutions of the equations governing many wave phenomena (e.g., scalar-wave,[1-6] Maxwell's,[3,7] Klein–Gordon[8] equations) have been reported recently. When compared with traditional monochromatic, continuous-wave (cw) solutions such as Gaussian or piston beams, these localized-wave (LW) solutions are characterized by extended regions of localization; i.e., their shapes and/or amplitudes are maintained over much larger distances than their cw analogs. These discoveries have prompted several extensive investigations into the possibility of using these LW solutions to drive finite-sized arrays, thereby launching fields having extended localization properties. This paper presents theoretical results and experimental evidence that confirm this LW effect.

The physics behind the LW effect is the coupling of the usually disjoint portions of phase space: space and frequency, due to the nonseparable nature of the LW solutions. The component wave forms and, therefore, their broad-bandwidth spectra, are strongly correlated to each other, a self-similarity property inherent to the LW solution. This spatial spectrum correlation leads to different pulses arriving from different locations with different, but correlated, frequency content; i.e., they arrive at the right place at the right time with the frequency components necessary to reconstruct the wave packet. A moving interference pattern forms at enhanced distances as the individual wave forms continue to propagate away from their sources. A new type of array is necessary to achieve this effect—each array element must be independently addressable so that the appropriate wave form can be radiated from it.

A preliminary acoustic experiment in water was reported[9] that exhibited successful localization of a transient, pencil beam of ultrasound launched from a LW-pulse-driven array. The array was linear, synthetic, and driven with the modified power spectrum (MPS) pulse

$$f(\mathbf{r},t) = \frac{1}{z_0 + i(z-ct)} \frac{1}{[(s/\beta)+a]^{\alpha}} e^{-bs/\beta}, \qquad (1)$$

where $s(\rho,z,t) = \rho^2/[z_0 + i(z-ct)] - i(z+ct)$ and the transverse distance $\rho = \sqrt{x^2+y^2}$. The parameters are $a = 1.0$ m, $\alpha = 1.0$, $b = 6.0\times 10^2$ m^{-1}, $\beta = 3.0\times 10^2$, and $z_0 = 4.5\times 10^{-4}$ m. The speed of sound in water is $c = 1.50\times 10^3$ m/s. The pencil beam generated by that array propagated several Gaussian Rayleigh distances before spreading. This comparison was based on the distance $L_G = \pi w_0^2/\lambda = 25.0$ cm, where $w_0 = 1.5$ cm was the initial waist of the beam; and the frequency $f = 0.53$ MHz ($\lambda = 0.283$ cm) was the $1/e$ roll-off point in the spectrum of the MPS pulse. Predictions indicated that further improvements were possible. Further synthetic array experiments have corroborated those predictions. A synthesized circular, planar array having a 3.0 cm radius was driven with the same MPS pulse; it produced a transient pencil beam that was localized out to $z \sim 150$ cm $= 6L_G$. The propagated beam waist was always narrower than the field generated by the same array driven with 0.5-, 1.0-, and 2.0-MHz cw tone bursts (truncated sine waves). This was true when the array was uniformly illuminated (an effective piston which produces a naturally focused beam) and when it was shaded with a spatial Gaussian taper (an initial transverse Gaussian with the same waist as the MPS pulse). The beam quality was better than the highest-frequency Gaussian and avoided the inherent near-field variations associated with a piston-generated field.

These results have led to a more definitive set of calculations and experiments to avoid some of the ambiguities that arise in comparing LW- and cw-driven arrays. In particular, the LW solutions are composed of broad-bandwidth wave forms, while traditional performance criteria are based upon cw, narrow-band concepts. There is no special frequency that can be selected to define, for instance, a Rayleigh distance when several different broadband spectra are involved. Nevertheless, performance comparisons are desirable. In the following we have chosen for the Rayleigh distance the definition $L_R = A/\lambda_R = Af_R/c$. The term A is the area of the array. The term f_R is obtained by integrating over frequency the array-weighted sum of the power spectra of the wave forms driving the array elements and defining f_R to be the frequency at which 87% of the total energy is accumulated (nominal $1/e^2$ point). This choice of L_R is more conservative than the original criterion since it encompasses the piston and Gaussian cw-driven array definitions, independent of the amplitude variations of the wave forms. Moreover, it involves a frequency larger than the average frequency driven into the array. Comparisons will be made with the same array driven with a conventional cw tone burst having a frequency of 0.5 MHz, which will be significantly above f_R. Another choice of f_R has been suggested to us by several researchers. For a broadband excitation of an array with a source function S whose spectrum is $\hat{S}$, the quantity f_{eff}, where

[a] Present address: Electromagnetics Laboratory, University of Arizona, ECE Bldg. 104, Tucscon, AZ 85721.

 0021-8979/90/246083-04$03.00

$$f_{\text{eff}}^2 = \frac{\int_A dA \int_{-\infty}^{\infty} dt\, |\partial_t S(\mathbf{r},t)|^2}{4\pi^2 \int_A dA \int_{-\infty}^{\infty} dt\, |S(\mathbf{r},t)|^2} = \frac{\int_A dA \int_{-\infty}^{\infty} d\omega |\omega \hat{S}(\mathbf{r},\omega)|^2}{4\pi^2 \int_A dA \int_{-\infty}^{\infty} d\omega |\hat{S}(\mathbf{r},\omega)|^2}, \quad (2)$$

could be used for f_R. This effective frequency value is appealing because it is related to the array-weighted variance of the spectra driven into the array and the array-weighted spectra of the field leaving the array face. The values of f_{eff} will be appropriately noted.

II. THEORY AND EXPERIMENT

A 25-element, 5×5, square array was fabricated which is 1.05 cm on a side and has 0.5-mm-diam disk elements (acoustic transducers) spaced on 2.5-mm centers. The small number of elements limits the number of cw configurations; there are too few elements for any effective shading or focusing. Six unique wave forms were designed for this array to achieve a ten-fold experiment, i.e., maintaining localization at least to $10\,L_R$. This was accomplished with a numerical simulation of the experiment.

Two versions of the numerical simulator were used. In one the resulting field was obtained by superposing the time signals radiated by each source directly in the time domain. In the other the field is generated by decomposing each input wave form into their Fourier components and then propagating each mode separately. The resulting field is obtained by superposing all of the Fourier components and inverse Fourier transforming. Even though this merely reproduced the same results predicted with the purely time-domain version, it demonstrates that the LW effect can also be handled from a strictly Fourier point of view. In the time domain we model the field received by a (point) transducer at $\mathbf{r}_m$ from the (point) transducers located at $\mathbf{r}_n$ in an array of N elements, each driven with the signal $S_n \equiv S(\mathbf{r}_n,t)$ as

$$g(\mathbf{r}_m,t) = \sum_{n=1}^{N} \frac{1}{2\pi c|\mathbf{r}_m - \mathbf{r}_n|} \partial_t^3 S(\mathbf{r}_n, t - |\mathbf{r}_m - \mathbf{r}_n|/c). \quad (3)$$

This model does not include the spatial pattern of each radiating element. Since the far field of each transducer in the constructed array at the frequencies of interest is reached near 1.0 cm, the model is valid after about two array lengths, i.e., 2.0 cm. On the other hand, this model includes not only the time effects of the radiating transducer, but also those of the receiving transducer. In particular, two of the time derivatives result from the movement of the faces of the transducers; the remaining one occurs from the disk-to-disk coupling. Although the resulting time derivatives have no effect on a cw field other than multiplication by a constant, they greatly impact the result of the LW fields because of the inherent spatial spectrum correlation (coupling of space and time). This three-time derivative model has been verified experimentally in other contexts.[10]

The array was simulated with 25 elements uniformly distributed over a 1.0-cm square area, giving $A = 1.0\ \text{cm}^2$. The driving wave forms were chosen from a modified version of the folded array scheme proposed in Ref. 3 and the MPS pulse (1). Explicitly, a radiating element at (x,y) is driven with the wave form

$$\begin{aligned} S(\rho,t) &= w(t) f(\rho, z=0, t) \quad (\rho = 0), \\ S(\rho,t) &= w(t)[f(\rho, z=0, t), \\ &\quad + (R/\rho)^4 f(R^2/\rho, z=0, t - t_d)] \quad (\rho \neq 0), \end{aligned} \quad (4)$$

where $R = (x_{\max}^2 + y_{\max}^2)^{1/2}$ is the maximum radius of the source locations in the array and the position-dependent delay time $t_d = \{[z_d^2 + (R^2/\rho)^2]^{1/2} - [z_d^2 + \rho^2]^{1/2}\}/c$, the constant delay distance being $z_d = 3.0\times10^{-2}$ m. If $h(t,\tau) = 0.42 - 0.50\cos[2.0\pi(t/\tau)] + 0.08\cos[4.0\pi(t/\tau)]$, the extra window function is $w(t) = 0$ for $t < -t_1$ and for $t > +t_4$; $w(t) = h(t,t_1)$ for $-t_1 < t < -t_2$ and $w(t) = h(t,t_4)$ for $+t_3 < t < +t_4$; and $w(t) = 1.0$ for $-t_2 \leq t \leq t_3$, where $t_1 = 6.0\times10^{-6}$ s, $t_2 = 3.0\times10^{-6}$ s, $t_3 = 0.5\times10^{-6}$ s, and $t_4 = 1.0\times10^{-6}$ s. The time window is included in the driving waveforms to remove the precursor wings characteristic of the regular MPS-driven arrays, hence to minimize specifically the amount of wasted energy in those wings. The pulses (3) were optimized by varying the constants in (3) and testing them in the simulator. The desired performance was obtained with the noted values. The value $f_R = 0.33$ MHz is obtained for the array and these driving functions. This gives $L_R = 2.2$ cm and the reference cw frequency 0.50 MHz $= 1.52 f_R$. Note that we found 50%, 63%, and 95% of the input energy, respectively, below 0.092, 0.135, and 0.50 MHz. If the $1/e$-fold (63%) point, a standard choice, were used, one would then have $L_R = 0.9$ cm. The value $f_{\text{eff}} = 0.33$ MHz was obtained numerically with the signal-processing code SIG.[11]

In the simulations the received energy $\mathscr{E}_r = \int |g|^2 dt$ is obtained by simply integrating over time the intensity of each received wave form. The total input energy $\mathscr{E}_{\text{in}} = \sum_{n=1}^{N} \int |S_n|^2 dt$ is obtained as the array-weighted sum of the energy associated with each driving function S_n. Since the driving functions in the LW case are all unipolar, the input energy of the cw case is taken to be twice the average

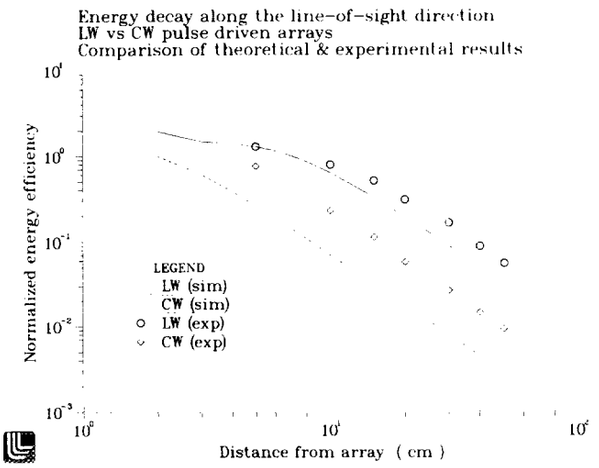

FIG. 1. The normalized energy efficiency of the theoretical and experimental beam fields generated from the LW- and 0.5-MHz cw-pulse-driven arrays are compared.

value per cycle. Note that one cycle of the reference 0.5-MHz cw case has a period approximately the same size as the entire LW pulse. We take as a measure of the energy efficiency of the arrays the ratio $\Gamma(z) = \mathscr{E}_r^{\max}(z)/\mathscr{E}_{\text{in}}$, where $\mathscr{E}_r^{\max}(z)$ is the maximum value within a 3.0-mm-radius disk (the size of the actual receiving transducer) centered on the line-of-sight axis a distance z from the array. This quantity is a direct measure of the performance of the LW- and cw-pulse-driven arrays. Plots of the predicted energy efficiency along the line-of-sight direction for the LW- and 0.5-MHz cw-driven arrays are shown as continuous curves in Fig. 1. Both curves have been normalized to the cw value at 2.0 cm. Consider the energy decay rate described by $1/r^{\epsilon}$. The cw case clearly reaches the $\epsilon = 2$ rate near 3.0 cm. In contrast, the results show that the energy decay of the LW-generated field attains the $\epsilon = 2$ rate near the 50–60-cm $\sim 25L_R$ range and has a rate with $\epsilon < 2$ before that distance.

To characterize the beam quality, we use the half width at half maximum (HWHM) of the beam energy profile: $\mathscr{E}_r$ as a function of transverse position. Plots of the predicted HWHM along the line-of-sight direction for the LW- and 0.5-MHz cw-driven arrays are shown as continuous curves in Fig. 2. The slopes of the LW and cw beam-spread curves are 0.0365 and 0.155, respectively. Their ratio is 4.25. The LW beam waist at $z = 30$ cm $\sim 15L_R$ is approximately double its value at $z = 5.0$ cm, where the pencil beam begins to spread; it is 3.80 times smaller than the waist of the 0.5-MHz cw beam there. Using the approximate cw criterion for the far-field HWHM, $w = z(\lambda/2D)$, the cw piston array required to obtain a similar beam width at 30.0 cm would be ~ 1.9 MHz $\sim 6f_R$.

The experiment is performed by digitizing the six driving functions, loading them into a programmable pulser, and multiplexing them to six digital-to-analog convertors (DACs), running at 100-ns sample intervals. The DACs then send the signals through amplifiers to the proper array elements. A 100-MHz clock was used to synchronize the system. The output of each amplifier was measured to ensure the proper signal level and frequency spectrum. The overall

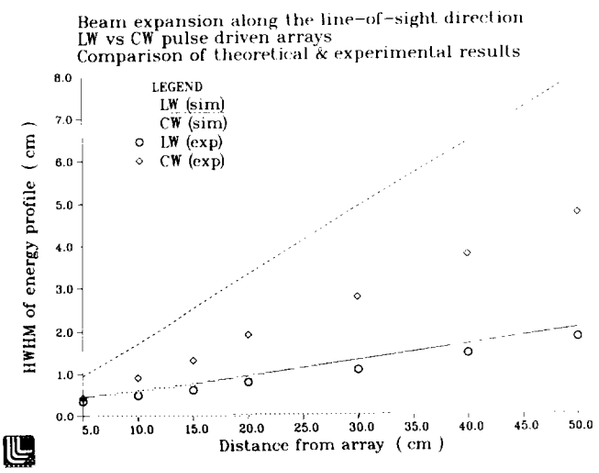

FIG. 2. The half width at half maximum of the energy profiles of the theoretical and experimental beam fields generated from the LW- and 0.5-MHz cw-pulse-driven arrays are compared.

electronics distort the pulses slightly so that the wave forms actually reaching the elements are modified versions of those given by (3). Precorrections were made to match the desired response as closely as the equipment allowed. In particular, the measured values are $f_{\text{eff}} \sim 0.29$ MHz and $f_R \sim 0.34$ MHz. The 0.5-MHz cw-driven array results from driving each element with a 0.5-MHz sinusoid, truncated to 16 μs in duration. The receiver is a single, standard 5.0-MHz, 3-mm-radius commercial transducer. Because of the size of the receive transducer, some averaging of the received beam is incurred. The beam is generated repetitively so that 1000 wave forms are collected and averaged to increase the signal-to-noise ratio. All measurements were digitized at a 20-ns sampling rate. We measure the beam at a given z distance from the array by sweeping the beam across the receiver. We sample it at 200 0.5-mm increments along a 10.0-cm distance perpendicular to the beam. We measure the instantaneous voltage seen by each element with a standard oscilloscope and measure the corresponding current with a Pearson probe. The input energy of both the LW and cw cases is then obtained by summing the time-integrated power seen by each element. Again, because the array radiates on both parts of the sine-wave cycle, we take the cw value to be twice its average value per cycle. The received energy is the time integral of the square of the measured voltage wave form. Both the transmitting and receiving transducers are resonant at 5.0 MHz, well above the frequencies of interest; no anomalous impedance resonances at lower frequencies were found.

The experimental beam characteristics for both the LW- and cw-pulse-driven arrays were obtained and compared with their predicted values. This included the overall pulse shape as well as the transmitted energy efficiency. We took measurements at $z = 5.0$, 10.0, 15.0, 20.0, 30.0, 40.0, and 50.0 cm. The measured values of $\Gamma(z)$ for the LW- and cw-pulse-driven arrays are given in Fig. 1. They are normalized so that the predicted and measured LW values at 5.0 cm coincide. The LW-pulse-driven array was approximately 6.00$\times$ more efficient than the 0.5-MHz cw-pulse-driven array at $z = 50$ cm, compared to the predicted value of 11.34. The LW field began to exhibit the $1/r^2$ decay rate between 30 and 40 cm, the cw field after 5.0 cm. The measured LW beam waist at $z = 30$ cm was 1.05 cm, 2.62 times smaller than the measured value of the 0.5-MHz cw beam there. The measured values of the HWMM of the beam profiles are given in Fig. 2. The final slopes of the beam-spread curves were 0.099 and 0.034 in the cw and LW cases, respectively. Their ratio was 2.91. The LW beam waist at $z = 30$ cm has slightly more than doubled its value at $z = 5.0$ cm; it is 2.62 times smaller than the waist of the 0.5-MHz cw beam there. The power spectrum of each of the received experimental wave forms was also obtained. Less than 25% of the low frequencies was lost from $z = 5$ to 50 cm, and so effectively the LW pencil beam has not lost its lowest frequencies even at $25L_R$. The absence of any significant frequency shedding corroborates the spatial spectrum correlation interpretation of the LW effect.

We believe the improvement of the experimental cw-driven-array case over the theoretical one is a result of the effective size of the array. It appears that the support face (a

dielectric membrane) which surrounds the transducers is also radiating in phase so that the effective area of the array is larger than the size defined by the elements. Several cycles of the cw pulse are radiated, giving the membrane a chance to resonate with the radiators. The LW case is simply on, then off. This membrane is rectangular; we found that the beams generated in both the LW and cw cases were slightly asymmetric in the directions corresponding to this shape. The modification of the cw beam was always much more apparent than with the LW beam. The results quoted here were for the larger beam dimensions; the beams in the orthogonal direction were narrower, corresponding to the larger membrane dimension. The rate of the beam expansion of the cw case in Fig. 2 is $\sim 1.42\times$ smaller than expected, indicating an effective array size ~ 1.57 cm. The membrane width in the corresponding direction is 1.60 cm, about a transducer size on either side of the radiating elements. The increased efficiency of the cw beam is slightly less than the corresponding increase in active area; the boundaries of the membrane appear to corrupt the cw field pattern, introducing some unexpected sidelobes which degrade the energy efficiency. In the LW case the slope indicates the size is ~ 1.07 cm, which corresponds nicely to the actual size of the array; and there is only an associated small increase over its predicted efficiency behavior. This active area aspect of the array could not be studied systematically since there is only one array of this type in existence (to our knowledge), and we do not wish to disassemble it.

Another notable feature of the LW pencil beam is the low level of its sidelobes. One could have driven this array with a 2.0-MHz cw signal to achieve a similar received energy and beamwidth. However, this would be achieved at the expense of efficiency, i.e., the sidelobe levels. Since the wavelength at 2.0 MHz is 0.075 cm, much smaller than the element separation, the array produces a beam with very large grating lobes when driven at this frequency. This effect was also confirmed experimentally. The grating lobes appear at the locations predicted from infinite-array theory with slightly decreased amplitudes because of the finite size of the actual array. The LW beam field is thus seen to be localized like the main beam of the 2.0-MHz case, but with the sidelobe levels of the 0.5-MHz case.

III. CONCLUSIONS

The LW transmission effect has now been verified with three different, but related experiments. The LW transient pencil beam field can be designed to outperform similar conventional cw fields in beam quality and/or delivered energy. It is quite robust even with a variety of losses and perturbations inherent in the experimental apparatus. In this case we achieved enhanced localization and energy transfer at an extended near-field distance of more than $10L_R$.

IV. ACKNOWLEDGMENTS

The authors are deeply indebted to Dale Fitting of the National Institute of Standards and Technology at Boulder, CO for fabricating and sharing with us the array used in this experiment. The authors are also deeply indebted to Professor Bill Cook of the University of Houston for his several careful readings of our original manuscripts and resulting suggestions, which led to an improved experiment and answers to his questions. As always, the authors acknowledge many stimulating conversations with Professor Yannis Besieris of VPI&SU. This work was performed in part by the Lawrence Livermore National Laboratory under the auspices of the U.S. Department of Energy under Contract No. W-7405-ENG-48.

[1] J. B. Brittingham, J. Appl. Phys. **54**, 1179 (1983).
[2] R. W. Ziolkowski, J. Math. Phys. **26**, 861 (1985).
[3] R. W. Ziolkowski, Phys. Rev. A **39**, 2005 (1989).
[4] A. M. Shaarawi, I. M. Besieris, and R. W. Ziolkowski, J. Math. Phys. **30**, 1254 (1989).
[5] P. D. Einziger and S. Raz, J. Opt. Soc. Am. A **4**, 3 (1987).
[6] E. Heyman and L. B. Felsen, J. Opt. Soc. Am. A **6**, 806 (1989).
[7] P. Hillion, J. Math. Phys. **28**, 1743 (1987).
[8] A. M. Shaarawi, I. M. Besieris, and R. W. Ziolkowski, J. Math. Phys. **31**, 2511 (1990).
[9] R. W. Ziolkowski, D. K. Lewis, and B. D. Cook, Phys. Rev. Lett. **62**, 147 (1989).
[10] B. D. Cook and D. K. Lewis, in *Proceedings of Ultrasonics International 87* (Butterworths, London, 1987), p. 947.
[11] D. Lager and S. Azevedo, LLNL Report No. UCID-19912, Rev. 1, Livermore, CA (1985).